FOCUS ISSUE OF SELECTED PAPERS FROM IMLB 2016 WITH INVITED PAPERS CELEBRATING 25 YEARS OF LITHIUM ION BATTERIES

Unraveling the Effects of Al Doping on the Electrochemical Properties of $LiNi_{0.5}Co_{0.2}Mn_{0.3}O_2$ Using First Principles

Mudit Dixit,* Boris Markovsky, Doron Aurbach,*** and Dan T. Major[z]**

Department of Chemistry and the Lise Meitner-Minerva Center of Computational Quantum Chemistry, Bar-Ilan University, Ramat-Gan 52900, Israel

One of the prevailing approaches to tune properties of materials is lattice doping with metal cations. Aluminum is a common choice, and numerous studies have demonstrated the ability of Al^{3+} doping to stabilize different positive electrode materials, such as Li[Ni-Co-Mn]O_2 (NCMs). Currently, an atomic level understanding of the stabilizing effect of Al doping in NCMs is limited. In this work, we investigate the effect of Al doping on Ni-rich-NCM-523 ($LiNi_{0.5}Co_{0.2}Mn_{0.3}O_2$). Our results suggest that Al stabilizes the structure of the cathode material via strong Al-O iono-covalent bonding due to a significant Al(s)-O(p) overlap, as well as significant charge transfer capabilities of Al. The calculated formation energies suggest that Al doping results in stabilization of partially lithiated states of NCM-523. On the other hand, calculated voltages indicate only a minor change in the voltage profiles as a function of the state-of-charge due to Al doping, and a modest increase in the Li diffusion barrier was observed. We note that high doping concentrations might mitigate the Li diffusion rates.

Manuscript submitted November 17, 2016; revised manuscript received December 19, 2016. Published January 7, 2017. This was Paper 835 presented at the Chicago, Illinois, Meeting of the IMLB, June 19–24, 2016. *This paper is part of the Focus Issue of Selected Papers from IMLB 2016 with Invited Papers Celebrating 25 Years of Lithium Ion Batteries.*

In recent decades, rechargeable batteries have demonstrated tremendous promise as alternate energy storage devices. In particular, Li-ion batteries (LIB) have revolutionized electronic devices, ranging from portable electronics to electric vehicles (EVs), due to their excellent power and energy density.[1] The bottleneck of LIB in terms of capacity and performance is often considered to be the nature of the positive electrodes (cathodes).[1–6] Among the cathode materials for LIB, layered transition metal (TM) oxides ($LiTMO_2$, TM = Ni, Co, Mn) are very promising candidates, and in particular $LiCoO_2$. However, in spite of the commercialization and wide use of $LiCoO_2$ in portable LIB, it suffers from several drawbacks. Key disadvantages include high cost and safety concerns associated with cobalt.[2–6] Other limitations of $LiCoO_2$ include low practical capacity (140 $mAhg^{-1}$) and oxygen loss on charge.[7–10] Consequently, in a quest to move beyond $LiCoO_2$, a new class of mixed transition metal oxides were designed, wherein Ni and Mn were introduced into the material (i.e. Li[$Ni_xCo_yMn_z$]O_2 or simply NCM).[11,12] The Ni-rich variants of these materials have emerged as the most promising low-cost and high capacity alternatives to the already mature $LiCoO_2$.[10,13,14,11] These Ni-rich materials show improved performance; however, the capacities and stabilities are still too low for practical commercialization for EVs.[12]

Key hurdles in the commercialization of these materials for EV applications are associated with oxygen release at high voltages and cation migration, which leads to structural transformations.[15,16] Recently, it has been demonstrated that oxygen loss and cation migration are concurrent events.[16,17]

To address these challenges, lattice doping of cations[18] has been adopted to improve the performance of these materials, and various cations were explored.[18–24] A particularly promising dopant for these materials is Al, although its effect is still not fully understood. Early theoretical studies proposed that Al substitution in $LiCoO_2$[25] and NCMs[26] could increase the intercalation potential, and these predictions were verified experimentally.[27] Various studies reported beneficial effects of Al doping on $LiCoO_2$ and $LiNiO_2$ and NCMs.[28–33]

To understand the stabilizing effect of Al doping in Ni-rich electrode materials, Guilmard et al. studied $Li_xNi_{0.89}Al_{0.16}O_2$ and $Li_xNi_{0.7}Co_{0.15}Al_{0.15}O_2$, and suggested Al^{3+} migration to tetrahedral sites as a possible mechanism for the suppression of layered-to-spinel transformation.[34,35] Delmas and co-workers studied Al doped NCM-424 ($Li_{1.04}Ni_{0.40}Co_{0.20-z}Mn_{0.40}Al_zO_2$), and found that Al doping reduces the reversible capacity, but significantly improves the thermal stability of the electrode in the de-intercalated state.[36] Al doping in Li-rich-Mn-rich NCMs has also improved the thermal stabilities of these materials.[37] In a detailed theoretical study, Dianat et al. studied the effect of Al doping on Li-Mn-Ni-O based cathode materials.[38] They reported that Al doping stabilizes the partially intercalated states, but increases the Li-diffusion barriers. Park et al. studied Al doping in $LiNiO_2$, and they found improved cycling behavior at high temperatures due to Al-doping. They attributed the stabilizing effect Al to the strong nature of Al-O bonds compared to Ni-O bonds.[33] In a recent study, Aurbach et al. demonstrated that Al doped $LiNi_{0.5}Co_{0.2}Mn_{0.3}O_2$ (NCM-523) possesses reduced capacity fading, less aging in the charged state, and has a more stable mean voltage behavior.[24]

Although considerable research has been performed on Al doping on different classes of materials, a sub-nanoscale level understanding of the effect of Al doping in NCMs is still far from clear. Such information could provide valuable insights, facilitating rational design of NCM-based superior cathode materials for LIB. In this study, we adopt a computational approach to investigate the effect of Al doping in NCM-523. To understand the effect of Al doping on NCM-523, we compute voltage profiles, electronic structure, oxygen binding energies and Li-ion diffusion profiles using density functional theory (DFT).

Computational methods.—DFT calculations were performed with the Vienna *ab-initio* simulation package (VASP).[39–41] The calculations employed the PBE exchange-correlation functional,[42] which is a generalized gradient approximation (GGA) method. In setting up the calculations, we assumed a spin polarized antiferromagnetic spin ordering. To represent the core electrons, plane-wave projector augmented wave (PAW) pseudo-potentials were used.[43] The kinetic energy cutoff was chosen to be 520 eV. The relaxed lattice parameters were computed using full spatial relaxation (both shape and volume

*Electrochemical Society Student Member.
**Electrochemical Society Member.
***Electrochemical Society Fellow.
[z]E-mail: majort@biu.ac.il

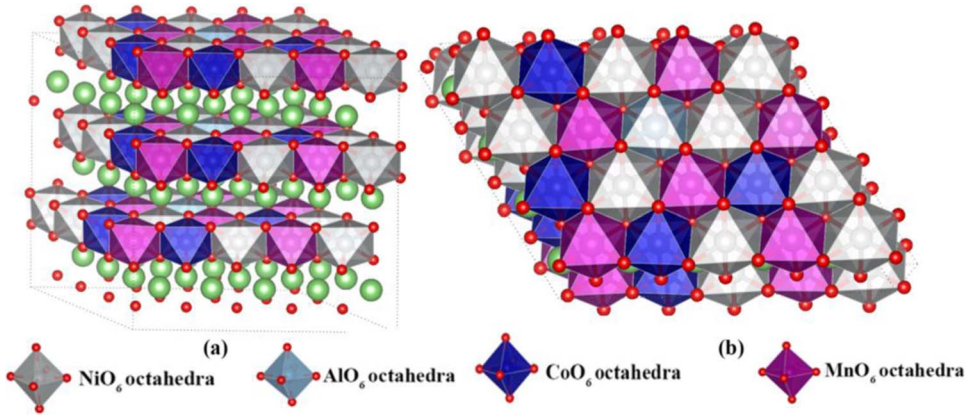

Figure 1. The relaxed supercell of $LiNi_{0.45}Co_{0.2}Mn_{0.3}Al_{0.05}O_2$, (a) side view of the supercell, (b) top view of the supercell showing the cation ordering. Li atoms are shown as green spheres.

relaxation) without any constraints, and the supercell geometries were considered minimized when the maximum force was found to be less than 0.01 eV/Å. All the calculations were performed on 5 × 4 supercells (60 formula units of the *R-3m* space group) of a α-$NaFeO_2$ type structure. Due to the large supercells employed (240 atoms) and the associated high computational cost, the calculations were performed using a modest 2 × 2 × 1 *k*-point grid set, which was generated by the Monkhorst–Pack scheme.[44] The values of the on-site coulomb interaction (U) potential were selected based on previous studies on a similar class of materials.[45,46] Specifically, we used the U = 5.96, 5.00 and 5.10 eV for Ni, Co and Mn, respectively. Dispersion corrections have been shown to be important in the prediction of lattice parameters of layered cathode materials.[47,48] In the current work, we incorporated dispersion corrections using the DFT+D3 approach, as implemented in the VASP code.[49]

In order to predict the preferred Al doping sites in the NCM-523 TM layers, we computed the substitution energies per Al atom as follows:

$$E_{subs-Ni} = \frac{1}{3}\Big[\{E_{Li_zNi_{0.5z-3}Co_{0.2z}Mn_{0.3z}Al_{0.05z}O_{2z}} + 3E_{LiNiO_2}\} - \{E_{Li_zNi_{0.5z}Co_{0.2z}Mn_{0.3z}O_{2z}} + 3E_{Li} + \frac{3}{2}E_{Al_2O_3} + \frac{3}{4}E_{O_2}\}\Big] \quad [1]$$

$$E_{subs-Co} = \frac{1}{3}\Big[\{E_{Li_zNi_{0.5z}Co_{0.2z-3}Mn_{0.3z}Al_{0.05z}O_{2z}} + 3E_{LiCoO_2}\} - \{E_{Li_zNi_{0.5z}Co_{0.2z}Mn_{0.3z}O_{2z}} + 3E_{Li} + \frac{3}{2}E_{Al_2O_3} + \frac{3}{4}E_{O_2}\}\Big] \quad [2]$$

$$E_{subs-Mn} = \frac{1}{3}\Big[\{E_{Li_zNi_{0.5z}Co_{0.2z}Mn_{0.3z-3}Al_{0.05z}O_{2z}} + 3E_{LiMnO_2}\} - \{E_{Li_zNi_{0.5z}Co_{0.2z}Mn_{0.3z}O_{2z}} + 3E_{Li} + \frac{3}{2}E_{Al_2O_3} + \frac{3}{4}E_{O_2}\}\Big] \quad [3]$$

where E represents the total energies of corresponding systems. For instance, $E_{Li_zNi_{0.5z-3}Co_{0.2z}Mn_{0.3z}Al_{0.05z}O_{2z}}$ and $E_{Li_zNi_{0.5z}Co_{0.2z}Mn_{0.3z}O_{2z}}$ represent the total energy of Al doped (at Ni sites) and undoped NCM-523, respectively. Our calculation models used the value of $z = 60$ (60 f.u. supercells).

The average intercalations potentials were computed assuming chemical equilibrium during the Li de-intercalation reaction, using the following equation:[50,51]

$$V = \left\{\frac{E_{Li_{x+dx}NCM} - E_{Li_xNCM}}{dx} - E_{Li_{bcc}}\right\} \quad [4]$$

where $E_{Li_{x+dx}NCM}$ and E_{Li_xNCM} represent the total energy (per formula unit) of the system before and after lithium extraction.

To account for oxygen evolution, we compute the oxygen binding energies (BE_O) using the PBE method. Specifically, the oxygen binding energy for NCM-523 is computed using following equation:

$$BE_O = \{E_{Li_zNi_{0.5z}Co_{0.2z}Mn_{0.3z}O_{2z-1}} + \tfrac{1}{2}E_{O_2}\} - \{E_{Li_zNi_{0.5z}Co_{0.2z}Mn_{0.3z}O_{2z}}\} \quad [5]$$

where $E_{Li_zNi_{0.5z}Co_{0.2z}Mn_{0.3z}O_{2z}}$, $E_{Li_zNi_{0.5z}Co_{0.2z}Mn_{0.3z}O_{2z-1}}$ and E_{O_2} represent the total energies of NCM-523, NCM-523 with one oxygen vacancy, and gaseous O_2, respectively.

Li-ion diffusion was investigated using the nudged elastic band (NEB)[52,53] method. In these calculations, the plane wave kinetic energy cutoff was set to 400 eV to reduce the computational cost. During the NEB calculations, the supercell lattice parameters were fixed to those obtained using PBE+U, but the on-site coulomb interaction U was not used for NEB calculations, as PBE+U method could results in mixing of the diffusion barrier with charge transfer barriers.[54] NEB calculations were performed in the fully intercalated limit. We note the dispersion corrections become important only in the low lithiation regime; therefore, dispersion corrections were not deemed essential and not included in these calculations.

Results and Discussion

Crystal structure of Al doped NCM-523.—Previous studies have shown that the lithiated mixed-TM based layered metal oxide materials exhibit limited in-plane ordering of TMs.[55–57] Various studies have confirmed ($\sqrt{3}$x$\sqrt{3}$)R30 type of ordering in these materials.[55–57] In a recent study, we obtained low-energy cationic ordering of NCM-523 using a multi-scale approach,[47] and for the current investigation of Al doped NCM-523, we adopted the cationic ordering of NCM-523 from our previous study.[47] One Ni ion was substituted with an Al ion in each layer (three ions in the supercell), resulting in the stoichiometric formula $LiNi_{0.45}Co_{0.2}Mn_{0.3}Al_{0.05}O_2$. All possible doping sites were studied at the DFT level of theory and the energetically most favorable structure of Al-doped NCM-523 (at Ni site) is presented in Fig. 1.

To elucidate the preferred substitution site for Al, we computed the substitution energy (E_{subs}) for Al-doping at all possible Ni, Co and Mn sites using the PBE functional. The most favorable structures were employed for the substitution energy calculation. The computed substitution energies (Fig. 2) suggest that Al doping is most preferred at Ni sites, followed by Co sites and least favorable at Mn sites. However, the substitution energies are found to be negative for all

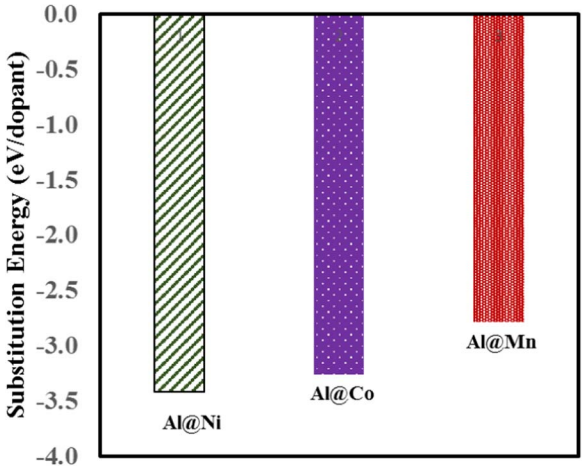

Figure 2. Calculated substitution energies for Al doping at metal (Ni, Co, Mn) sites in NCM-523.

TMs, suggesting that Al-doping might be possible at all TM sites. These findings are in agreement with our previous study, although the magnitudes of the substitution energies were found to be lower in the current case due different reference states for the transition metals (ground-state metal oxides were taken as the reference state as opposed to the bulk metals in our previous study).[24]

Fig. 3 highlights the calculated lattice parameters of metal-doped NCM-523. We obtain reasonable agreement between the calculated ($a = 2.89, c = 14.29$) and experimental ($a = 2.86, c = 14.23$) parameters for the pristine state (x = 1) using the PBE functional.[24] However, for the fully de-intercalated state, the *c* lattice parameters are found to be higher than expected.[24,47] This increase was recently attributed to deficiency of the dispersion treatment in PBE, which becomes significant in the low intercalated limit.[48] As seen in our previous studies on NCM-523 and NCM-622, the inclusion of dispersion corrections results in an expected drop in the *c* lattice parameters at low lithiation (Fig. 3).[47,48,58] These results emphasize the importance of adding dispersion corrections in the structural study of layered NCMs at low lithiation levels.

Electronic structure of undoped and Al-doped materials.—Fig. 4 presents the density of states (DOS) computed with both PBE and PBE+U methods. Interestingly, the DOS using the PBE+U method with the U values adopted from single TM oxides (Figure 4b) suggests a large contribution of oxygen ions near the Fermi level, while the TM *d*-states are shifted to energies significantly below the Fermi level. Such positioning of TM-*d* and oxygen-*p* states is at odds with the electrochemical activity ascribed to TM redox. On the other hand

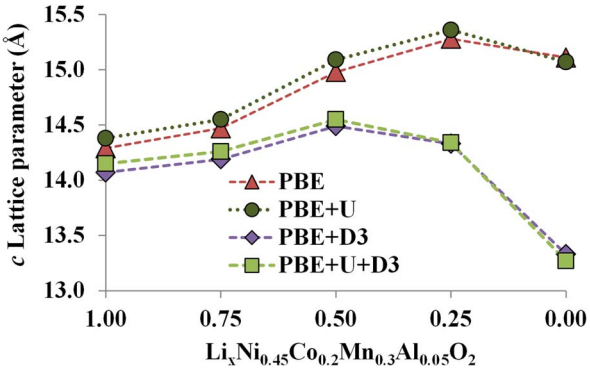

Figure 3. Calculated *c* lattice parameters (Å) of Al doped NCM-523 as a function of state of charge.

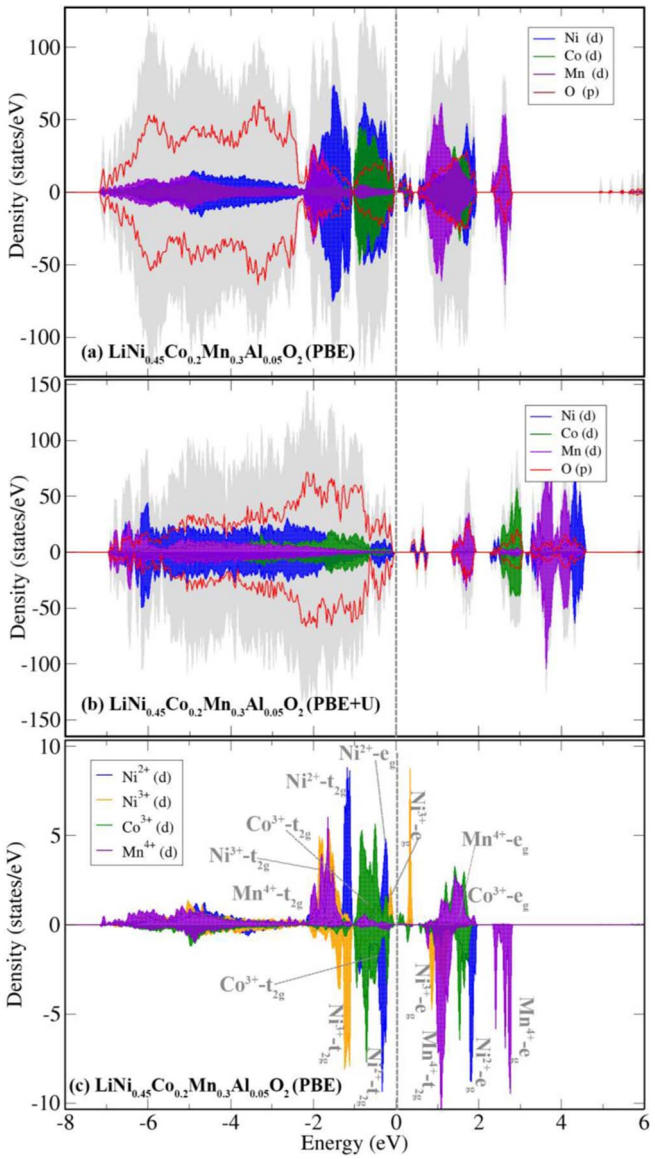

Figure 4. Density of states for $LiNi_{0.45}Co_{0.2}Mn_{0.3}Al_{0.05}O_2$ using (a) PBE (b) PBE+U. (c) Single ion projected density of states for $LiNi_{0.45}Co_{0.2}Mn_{0.3}Al_{0.05}O_2$ using PBE.

PBE predicts that the *d*-states of the TM are located near the Fermi level (Figs. 4b, 4c). The electronic structure computed by the PBE functional explains the electrochemical activity due to cationic redox of NCM-523, and is in agreement with the suggested electronic structure for this class of materials.[59,60] In spite of the known self-interaction error of the PBE method, it often predicts an electronic structure of NCMs in good agreement with experiments[61] (i.e. relative positions of the TM *d*- and oxygen *p*-states). Additionally, PBE accurately predicts voltage trends,[47,62–65] defect formation energies[66] and TM layer stacking sequences[67] of layered TM oxide materials. Adding a Hubbard correction parameter (i.e. PBE+U) corrects self-interaction errors in the functional, and hence one might expect to get a correct description of oxides and lithiated layered oxides. However, the magnitude of the optimal U parameter depends on the electron correlation in the material being studied, and this electron correlation changes as a function of lithiation (i.e. TM oxidation state) of layered TM oxides.[68,69] For instance, for $LiCoO_2$ the U value which gives correct electronic structure (U∼2.9) could not predict the correct average voltages. Indeed, to accurately predict the average voltage a higher U

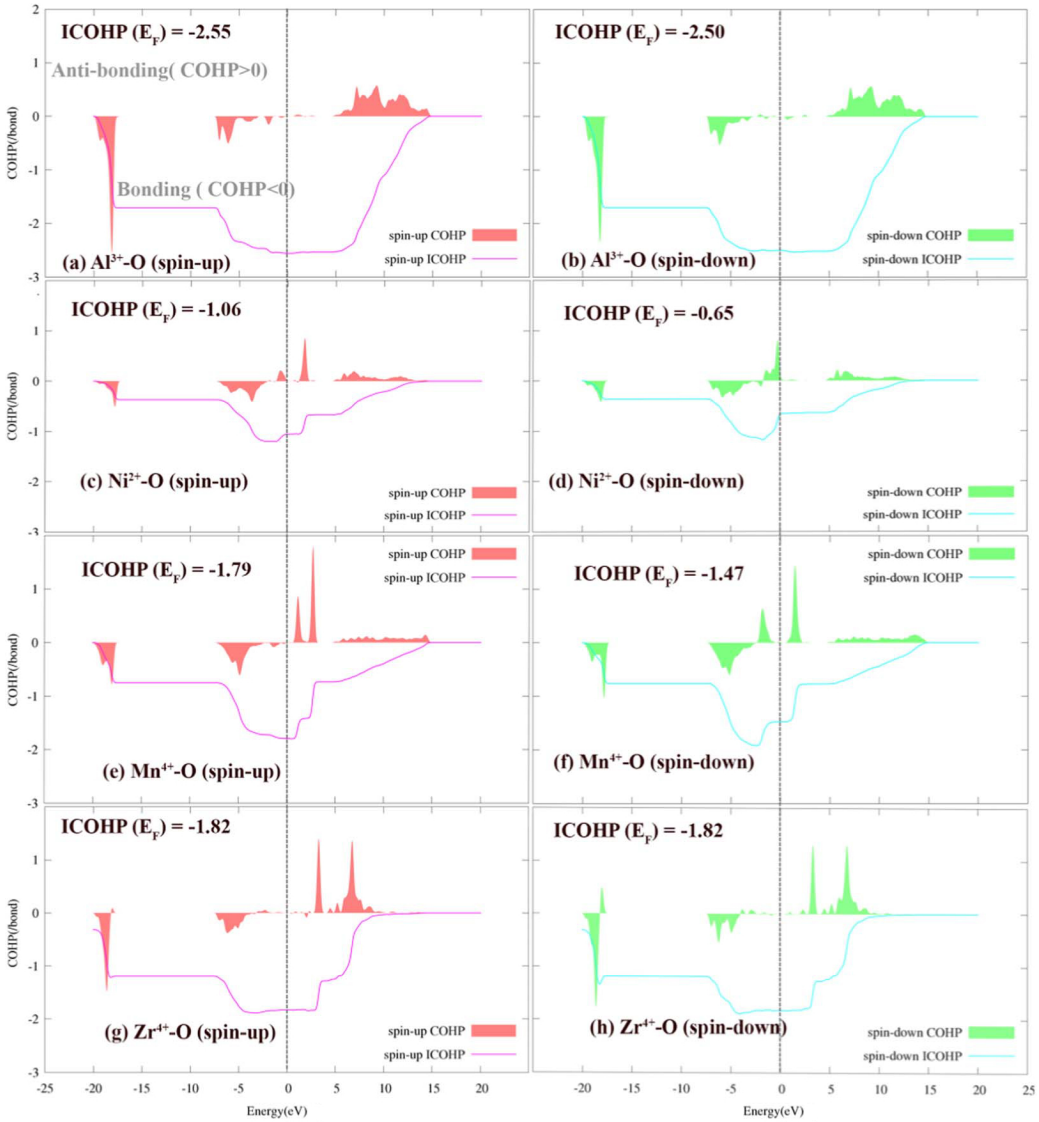

Figure 5. Projected and integrated COHP using PBE for (a) Al^{3+}-O bonds spin-up (b) Al^{3+}-O bonds spin-down (c) Ni^{2+}-O bonds spin-up (d) Ni^{2+}-O bonds spin-down (e, f) Mn^{4+}-O bonds in Al doped NCM-523. Projected and integrated COHP Zr^{4+}-O bonds in Zr-doped NCM-523 for (g) spin-up (h) spin-down.

value is often selected (U = 4.9).[70,71] Therefore, further analysis was done with the PBE method only.

The formal oxidation states of transition metals are often estimated based on the calculated magnetic moments and projected DOS (PDOS). The PDOS (Fig. 4) suggests that Ni ions have two distinct electronic configurations, corresponding to $t_{2g}^6e_g^2$ and $t_{2g}^6e_g^1$. Inspection of both the magnetic moments and PDOS suggest that in the pristine state of Al-doped NCM-523 Ni exists in both +2 and +3 formal oxidation states, similar to what observed for NCM-523[47] and NCM-622[58]. For the Co-ions, we predict a +3 valence state with the electronic configuration of $t_{2g}^6e_g^0$ based on the PDOS and the absence of a magnetic moment. A +4 valence state for the Mn ions ($t_{2g}^3e_g^0$) is suggested by the magnetic moments (>2μB) and spin-singly occupation of the t_{2g} states. We note that minute Al-doping (5%) does not change the electronic structure significantly.

Stabilizing effect of Al.—To address the intriguing stabilizing effect of low Al-doping, we investigated the Bader charges,[72] crystal orbital Hamilton populations (COHP),[73] and oxygen binding energies. For comparison, we also considered high charge (Zr^{4+}) dopants in NCM-523, in addition to Al^{3+}. The absolute average Bader charge on oxygen (Table I) in the dopant octahedra (MO_6; M = Ni, Al, Zr) follows the order: undoped NCM-523 < Al-doped NCM-523 < Zr-doped NCM-523. Interestingly, Al with a +3 formal charge transfers a similar amount of charge as Zr^{4+}. These results suggest that Al effectively transfers its electrons to the oxygen, thereby increasing the absolute oxygen charge. Previously, it was suggested that a higher absolute oxygen charge results in greater oxygen binding energy.[46] Our

Table I. The calculated Bader charges in metal doped NCM-523 using PBE method.

System	Average charge on oxygen (e)[a]	Charge on dopant (e)	Oxygen binding energy (eV)
Undoped NCM-523	−1.12	1.19 (Ni)	2.61
Al-doped NCM-523	−1.30	2.46	3.47
Zr-doped NCM-523	−1.37	2.49	3.78

[a]Averaged over dopant octahedra.

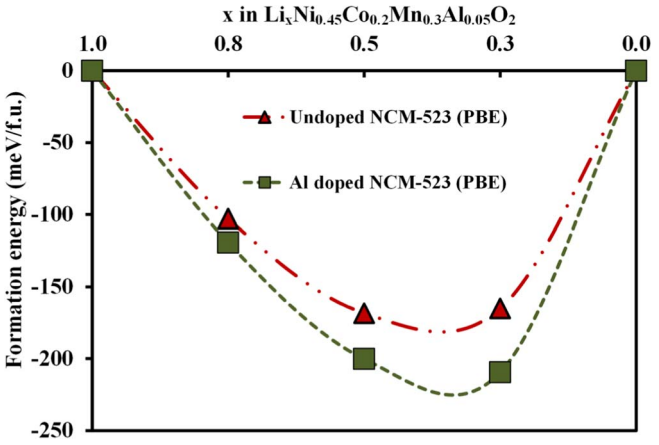

Figure 6. Calculated formation energies of Al doped and undoped NCM-523 using the PBE method.

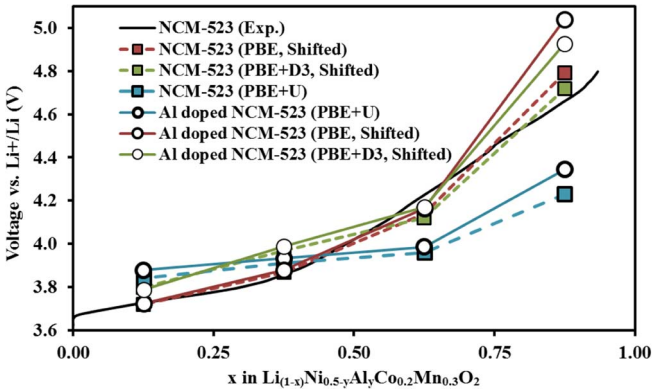

Figure 7. Calculated voltage profiles for Al-doped NCM-523 at different delithiation levels. The calculated voltages obtained using PBE and PBE+D3 were rigidly shifted up by 0.9 eV and 0.6 eV, respectively. The experimental voltage profile of NCM-523 are taken from Ref. 77. To plot the experimental profile a specific capacity of 250 mA h g^{-1} was considered in the fully delithiated state. y = 0 for un-doped NCM-523 and y = 0.05 for Al-doped NCM-523.

calculated oxygen binding energies further verifies this finding (Table I).

COHP is very useful in understanding chemical bonding in solids. Fig. 5 shows the bond-projected COHP (pCOHP) for M-O bonds in Al-doped NCM-523 (Zr-O in Zr-doped NCM-523). Inspection of the Al-O pCOHP shows a high integrated COHP (ICOHP) of -2.5/bond; this suggests strong Al-O bonding, and is likely due to Al(s)-O(p) hybridization. We note that such a strong overlap was not found for other metals. A significant charge transfer with considerable orbital overlap suggests an iono-covalent nature of the Al-O bond.[74,75]

The inspection of the ICOHP for the various dopants suggest that the order of bonding overlap is Al^{3+}-O > Zr^{4+}-O > Mn^{+4}-O > Ni^{+2}-O. In conclusion, we find high oxygen binding energy and high ICOHP, which both point to strong Al-O bonding. Such strong iono-covalent Al-O bonds could effectively stabilize the NCM lattice as a result of doping.

Effect of Al doping on electrochemical stability.—One of the crucial factors in determining the performance of a battery is electrochemical stability. The instability of partially delithiated states result in deleterious capacity fading. During Li de-intercalation, the oxidation states of transition metals change, which often lead to structural instability. Thermodynamic characterization of the stability of partially delithiated states is given by the formation energy (E_f):

$$E_f = E(Li_xMO_2) - xE(LiMnO_2) - (1-x)E(MO_2) \quad [6]$$

$E(Li_xMO_2)$, $E(MO_2)$ and $E(LiMO_2)$ are the total energies of partially delithated, fully delithated and fully lithated states, respectively.

The formation energy of the partially delithiated states (Fig. 6) provides the relative stability of a given state with respect to the phase-separated states. Negative formation energy suggests a solid solution behavior whereas positive formation energy suggests a phase separation. Fig. 6 presents the formation energy of Al-doped and undoped NCM-523. Interestingly, the absolute formation energies of the Al doped material are greater than that of the undoped material, suggesting that Al doping stabilizes the partially delithiated state. We also note that both Al-doped and undoped materials have negative formation energies during the course of delithaition. These findings are in line with the recent theoretical study by Dianat et al. on Li-Ni-Mn-O based materials.[38] Our results are also in accordance with our previous experimental work, which shows smooth voltage profiles (solid solution) for both Al-doped and undoped NCM-523, suggesting solid solution behavior.[24]

Effect of Al doping on de-intercalation voltage profiles.—One of the primary properties of cathode materials is voltage. Therefore, the effect of dopant on the voltages is crucial. The computed voltage profiles (Fig. 7) for Al-doped NCM-523 using PBE (up shifted) and the PBE+D3 (up shifted) is found to be similar to the experimental and computed voltage profiles of undoped NCM-523.[47] These results are also in agreement with our recent experimental study on Al doped NCM-523, which demonstrated similar voltage profiles for undoped and Al doped NCM-523.[24] As noted recently, the PBE+U method is not able to reproduce the voltage profiles of NCMs.[47,62,76] The inability of the PBE+U method (with U values of lithiated single TM oxides) to predict voltage profiles could be due several factors, such as change in electron correlation of NCMs as a function of Li de-intercalation, as mentioned above (i.e. different U values are needed for different states of charge because of change in the formal oxidation states of TMs).[47] It is noteworthy that investigation of the transferability of the U values of single-TM oxides to the multi-TM oxides (e.g. NCM) at different states of charge, might be necessary for the application of GGA+U in voltage profile calculations. Interestingly, we note that the calculated voltages of the undoped materials are slightly higher than that of the undoped material. This finding is also in line with previous experimental data.[24]

Effect of Al doping on Li diffusion.—Fast Li-ion diffusion is an important requirement for high power density LIB cathode materials. Sluggish Li diffusion kinetics results in loss of LIB power density and often leads to undesired phase transitions. In layered cathode materials two main mechanisms for Li diffusion have been proposed.[78] These mechanisms are dubbed oxygen dumbbell hops (ODH) and tetrahedral site hops (TSH), based on the type of transition state (TS) involved.[78] Near the fully lithiated limit, Li diffusion occurs primarily via an ODH pathway.[77] To understand the effect of Al-doping on Li diffusion, we investigate the Li hopping mechanism from one Li octahedral site to another vacant Li octahedral site, via an ODH pathway. To compute the Li diffusion profile we created a single Li vacancy (i.e. fully lithiated limit), and the Li diffusion from the neighboring octahedral site was investigated using the ODH pathway.

The calculated Li diffusion barrier (Fig. 8) near the Al-doped site in doped NCM-523 (0.63 eV) is found to be significantly higher than that of undoped NCM-523 (0.50 eV). This is possibly due to greater repulsive interactions between Li^+-Al^{3+} ions at the TS of Li diffusion in the Al-doped material relative to the undoped material (Li^+-Ni^{2+} repulsion). These results suggest that a large amount of Al-doping might mitigate Li diffusion. Since the '*c*' lattice parameter was not found to be altered significantly, the increase in Li-diffusion barrier on doping is expected to be a local effect. Indeed, we find that Li-diffusion barrier in the vicinity of the second-nearest neighboring TM (Ni, 0.53 eV) was found to be only slightly higher than that of the undoped material. Therefore, we suggest that the net Li diffusion rates

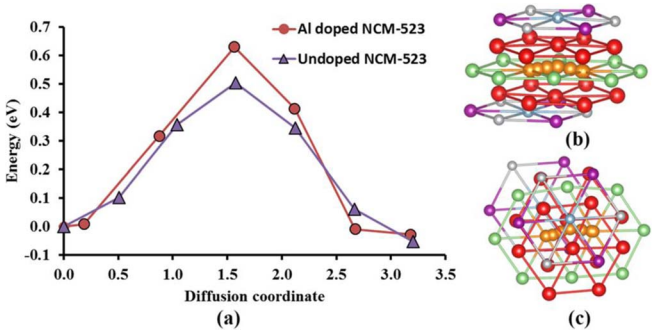

Figure 8. Li diffusion profile for undoped and Al-doped NCM-523 using PBE. (a) The NEB energy profiles, (b) top view of ODH path, (c) side view of ODH path. Color code for spheres: green-Li atoms, grey-Ni atoms, violet-Mn atoms, red-oxygen atoms. Orange spheres indicate NEB images for the Li atoms. For the sake of clarity, only the Li-migration part of the system is shown. Diffusion coordinate is given in angstrom.

in minutely Al-doped materials might be similar to that of the undoped material.

Conclusions

In this work, we studied the effect Al-doping in NCM-523 on a range of properties relevant to electrochemistry using first principle DFT calculations. Our results suggest that the stabilizing effect of Al is mainly due to strong Al-O iono-covalent bonding via Al(s)-O(p) overlap with a high degree of charge transfer from Al to oxygen. These strong Al-O bonds might provide stability in partially delithiated cathode states. Calculations of formation energies also indicated greater stabilization of partially lithiated states on Al doping. Furthermore, only a slight increase in the voltage profiles was observed on Al doping. Inspection of ion-diffusion profiles, suggests that Al-doping increases the Li diffusion barrier primarily near the dopant site. However, this effect is less pronounced for Li-diffusion further removed from the site of doping, suggesting that low doping levels (5 atomic percent) are unlikely to affect bulk Li-diffusion properties. Our findings on Al doping in NCM-523 could be general for other positive electrode materials.

Acknowledgments

This work was supported by the Israel Science Foundation (grant no. 2797/11) and Israel National Research Center for Electrochemical Propulsion (INREP) consortium.

References

1. V. Etacheri, R. Marom, R. Elazari, G. Salitra, and D. Aurbach, *Energ Environ Sci*, **4**, 3243 (2011).
2. J. B. Goodenough and Y. Kim, *Chem. Mater.*, **22**, 587 (2009).
3. A. Manthiram, *J. Phys. Chem. Lett.*, **2**, 176 (2011).
4. M. M. Thackeray, C. Wolverton, and E. D. Isaacs, *Energy Environ. Sci.*, **5**, 7854 (2012).
5. G. Ceder, *Mrs Bulletin*, **35**, 693 (2010).
6. M. S. Islam and C. A. Fisher, *Chem. Soc. Rev*, **43**, 185 (2014).
7. K. Mizushima, P. Jones, P. Wiseman, and J. Goodenough, *Materials Research Bulletin*, **15**, 783 (1980).
8. J. N. Reimers and J. R. Dahn, *J. Electrochem. Soc.*, **139**, 2091 (1992).
9. Y. Shao-Horn, L. Croguennec, C. Delmas, E. C. Nelson, and M. A. O'Keefe, *Nat. Mater.*, **2**, 464 (2003).
10. R. V. Chebiam, F. Prado, and A. Manthiram, *Chem. Mater.*, **13**, 2951 (2001).
11. Z. Lu, D. MacNeil, and J. Dahn, *Electrochem. Solid State Lett.*, **4**, A200 (2001).
12. T. Ohzuku and Y. Makimura, *Chem. Lett.*, **30**, 642 (2001).
13. M. S. Whittingham, *Chem. Rev.*, **104**, 4271 (2004).
14. C. S. Yoon, M. H. Choi, B.-B. Lim, E.-J. Lee, and Y.-K. Sun, *J. Electrochem. Soc.*, **162**, A2483 (2015).
15. W. Liu, P. Oh, X. Liu, M.-J. Lee, W. Cho, S. Chae, Y. Kim, and J. Cho, *Angew. Chem. Int. Ed.*, **54**, 4440 (2015).
16. J. Yang and Y. Xia, *ACS Appl. Mater. Interfaces*, **8**, 1297 (2016).
17. S.-M. Bak, K.-W. Nam, W. Chang, X. Yu, E. Hu, S. Hwang, E. A. Stach, K.-B. Kim, K. Y. Chung, and X.-Q. Yang, *Chem. Mater.*, **25**, 337 (2013).
18. J. W. Fergus, *J. Power Sources*, **195**, 939 (2010).
19. Y. Zhang and C.-Y. Wang, *J. Electrochem. Soc.*, **156**, A527 (2009).
20. M. Mladenov, R. Stoyanova, E. Zhecheva, and S. Vassilev, *Electrochem. Commun.*, **3**, 410 (2001).
21. E.-S. Lee and A. Manthiram, *J. Mater. Chem. A*, **1**, 3118 (2013).
22. Y.-S. He, L. Pei, X.-Z. Liao, and Z.-F. Ma, *J. Fluorine Chem.*, **128**, 139 (2007).
23. L. Croguennec, J. Bains, M. Ménétrier, A. Flambard, E. Bekaert, C. Jordy, P. Biensan, and C. Delmas, *J. Electrochem. Soc.*, **156**, A349 (2009).
24. D. Aurbach, O. Srur-Lavi, C. Ghanty, M. Dixit, O. Haik, M. Talianker, Y. Grinblat, N. Leifer, R. Lavi, D. T. Major, and B. Markovsky, *J. Electrochem. Soc.*, **162**, A1014 (2015).
25. G. Ceder, Y. M. Chiang, D. R. Sadoway, M. K. Aydinol, Y. I. Jang, and B. Huang, *Nature*, **392**, 694 (1998).
26. S.-K. Hu, T.-C. Chou, B.-J. Hwang, and G. Ceder, *J. Power Sources*, **160**, 1287 (2006).
27. Y. I. Jang, B. Huang, H. Wang, D. R. Sadoway, G. Ceder, Y. M. Chiang, H. Liu, and H. Tamura, *J. Electrochem. Soc.*, **146**, 862 (1999).
28. S.-T. Myung, N. Kumagai, S. Komaba, and H.-T. Chung, *Solid State Ion.*, **139**, 47 (2001).
29. J. Kim, B. Kim, Y. Baik, P. Chang, H. Park, and K. Amine, *J. Power Sources*, **158**, 641 (2006).
30. T. Amriou, A. Sayede, B. Khelifa, C. Mathieu, and H. Aourag, *J. Power Sources*, **130**, 213 (2004).
31. H. Cao, B. Xia, N. Xu, and C. Zhang, *J. Alloy. Comp.*, **376**, 282 (2004).
32. F. Zhou, X. Zhao, Z. Lu, J. Jiang, and J. Dahn, *Electrochem. Commun.*, **10**, 1168 (2008).
33. S. H. Park, K. S. Park, Y. K. Sun, K. S. Nahm, Y. S. Lee, and M. Yoshio, *Electrochim. Acta*, **46**, 1215 (2001).
34. M. Guilmard, L. Croguennec, and C. Delmas, *Chem. Mater.*, **15**, 4484 (2003).
35. M. Guilmard, L. Croguennec, D. Denux, and C. Delmas, *Chem. Mater.*, **15**, 4476 (2003).
36. L. Croguennec, J. Bains, J. Bréger, C. Tessier, P. Biensan, S. Levasseur, and C. Delmas, *J. Electrochem. Soc.*, **158**, A664 (2011).
37. Z. Li, N. A. Chernova, J. Feng, S. Upreti, F. Omenya, and M. S. Whittingham, *J. Electrochem. Soc.*, **159**, A116 (2011).
38. A. Dianat, N. Seriani, M. Bobeth, and G. Cuniberti, *J. Mater. Chem. A*, **1**, 9273 (2013).
39. G. Kresse and J. Hafner, *Phys. Rev. B*, **47**, 558 (1993).
40. G. Kresse and J. Hafner, *Phys. Rev. B*, **49**, 14251 (1994).
41. G. Kresse and J. Furthmüller, *Comp. Mater. Sci.*, **6**, 15 (1996).
42. J. P. Perdew, K. Burke, and M. Ernzerhof, *Phys. Rev. Lett.*, **77**, 3865 (1996).
43. P. E. Blöchl, *Phys. Rev. B*, **50**, 17953 (1994).
44. H. J. Monkhorst and J. D. Pack, *Phys. Rev. B*, **13**, 5188 (1976).
45. F. Zhou, M. Cococcioni, K. Kang, and G. Ceder, *Electrochem. Commun.*, **6**, 1144 (2004).
46. P. Xiao, Z. Deng, A. Manthiram, and G. Henkelman, *J. Phys. Chem. C*, **116**, 23201 (2012).
47. M. Dixit, M. Kosa, O. S. Lavi, B. Markovsky, D. Aurbach, and D. T. Major, *Phys. Chem. Chem. Phys.*, **18**, 6799 (2016).
48. M. Aykol, S. Kim, and C. Wolverton, *J. Phys. Chem. C*, **119**, 19053 (2015).
49. S. Grimme, J. Antony, S. Ehrlich, and H. Krieg, *J. Chem. Phys.*, **132**, 154104 (2010).
50. W. R. McKinnon, 'Insertion electrodes I: Atomic and electronic structure of the hosts and their insertion compounds', in Bruce, P.G. (ed.), Solid State Electrochemistry, pp. 163–198, Cambridge University Press, Cambridge (1994).
51. M. Aydinol, A. Kohan, G. Ceder, K. Cho, and J. Joannopoulos, *Phys. Rev. B*, **56**, 1354 (1997).
52. G. Henkelman, B. P. Uberuaga, and H. Jónsson, *J. Chem. Phys.*, **113**, 9901 (2000).
53. G. Mills, H. Jónsson, and G. K. Schenter, *Surf. Sci.*, **324**, 305 (1995).
54. S. P. Ong, V. L. Chevrier, G. Hautier, A. Jain, C. Moore, S. Kim, X. Ma, and G. Ceder, *Energ Environ Sci*, **4**, 3680 (2011).
55. F. Weill, N. Tran, L. Croguennec, and C. Delmas, *J. Power Sources*, **172**, 893 (2007).
56. D. Zeng, J. Cabana, J. Bréger, W.-S. Yoon, and C. P. Grey, *Chem. Mater.*, **19**, 6277 (2007).
57. L. Cahill, S.-C. Yin, A. Samoson, I. Heinmaa, L. Nazar, and G. Goward, *Chem. Mater.*, **17**, 6560 (2005).
58. F. Schipper, M. Dixit, D. Kovacheva, M. Talianker, O. Haik, J. Grinblat, E. M. Erickson, C. Ghanty, D. T. Major, B. Markovsky, and D. Aurbach, *J. Mater. Chem. A*, **4**, 16073 (2016).
59. R. Chebiam, F. Prado, and A. Manthiram, *Chem. Mater.*, **13**, 2951 (2001).
60. C. M. Julien, A. Mauger, K. Zaghib, and H. Groult, *Inorganics*, **2**, 132 (2014).
61. G. Cherkashinin, M. Motzko, N. Schulz, T. Späth, and W. Jaegermann, *Chem. Mater.*, **27**, 2875 (2015).
62. I. M. Markus, F. Lin, K. C. Kam, M. Asta, and M. M. Doeff, *J. Phys. Chem. Lett.*, **5**, 3649 (2014).
63. B. Hwang, Y. Tsai, D. Carlier, and G. Ceder, *Chem. Mater.*, **15**, 3676 (2003).
64. A. Osnis, M. Kosa, D. Aurbach, and D. T. Major, *J. Phys. Chem. C*, **117**, 17919 (2013).
65. D.-H. Seo, A. Urban, and G. Ceder, *Phys. Rev. B*, **92**, 115118 (2015).
66. M. S. Park, *Phys. Chem. Chem. Phys.*, **16**, 16798 (2014).
67. M. D. Radin and A. Van der Ven, *Chem. Mater.*, **28**, 7898 (2016).
68. S. Kawasaki, T. Motohashi, K. Shimada, T. Ono, R. Kanno, M. Karppinen, H. Yamauchi, and G.-q. Zheng, *Phys. Rev. B*, **79**, 220514 (2009).

69. S. Mazumdar and R. T. Clay, *Physica Status Solidi (B)*, **249**, 995 (2012).
70. D. Ensling, A. Thissen, S. Laubach, P. C. Schmidt, and W. Jaegermann, *Phys. Rev. B*, **82**, 195431 (2010).
71. J. A. Santana, J. Kim, P. Kent, and F. A. Reboredo, *J. Chem. Phys.*, **141**, 164706 (2014).
72. W. Tang, E. Sanville, and G. Henkelman, *J. Phys. Condens. Matter*, **21**, 084204 (2009).
73. V. L. Deringer, A. L. Tchougréeff, and R. Dronskowski, *J. Phys. Chem. A*, **115**, 5461 (2011).
74. M. Digne, P. Sautet, P. Raybaud, P. Euzen, and H. Toulhoat, *J. Catal.*, **226**, 54 (2004).
75. C. Arrouvel, B. Diawara, D. Costa, and P. Marcus, *J. Phys. Chem. C*, **111**, 18164 (2007).
76. D.-H. Seo, A. Urban, and G. Ceder, *arXiv preprint arXiv:1507.08768* (2015).
77. Y. Wei, J. Zheng, S. Cui, X. Song, Y. Su, W. Deng, Z. Wu, X. Wang, W. Wang, M. Rao, Y. Lin, C. Wang, K. Amine, and F. Pan, *J. Am. Chem. Soc.*, **137**, 8364 (2015).
78. A. Van der Ven and G. Ceder, *Electrochem. Solid State Lett.*, **3**, 301 (2000).